# Dynamic Impact Tests on Lithium-Ion Cells

Thomas Kisters[a], Elham Sahraei[b,c], Tomasz Wierzbicki[b]

*a)Fraunhofer Ernst-Mach-Institute, Am Klingelberg 1, 79588 Efringen-Kirchen, Germany*

*e-mail: thomas.kisters@emi.fraunhofer.de*

*phone: +49 7628 9050687*

*fax: +49 7628 90501687*

*b) Massachusetts Institute of Technology, Cambridge, MA, USA*

*c) George Mason University, Fairfax, VA, 22030*

**Abstract**

This paper reports on dynamic abuse tests on Li-ion cells, namely investigations on local indentation/intrusion into these cells. Two different types of cells have been investigated, pouch cells and elliptic cells. The elliptic cells were tested in two different states, with and without liquid electrolyte. The cells have been loaded by a hemispherical punch with a diameter of 12.7 mm with velocities between 0.01 mm/s and 5000 mm/s. Intrusion force, intrusion depth and velocity, and cell voltage were measured with high time-resolution during the intrusion process.

Significant changes in critical force were detected over the span of tested velocities. The critical force increased with an increase in test speed for the elliptic cells, while it decreased for the pouch cells. There were also differences associated with the presence of the electrolyte. These findings are of great importance especially for automotive applications where Li-ion battery packs are used in Hybrid or Electric Vehicles where intrusion at dynamic speeds is one of the main failure modes during a crash. The paper describes the experimental setup and test results in detail and discusses the implications.

**Keywords:** internal short circuit, dynamic material properties, mechanical abuse, lithium ion cell, pouch cell

## 1. Introduction

Electrical energy storage devices are gaining increasing importance for propulsion technology as well as temporary energy storage. Much effort, accordingly, is put into increasing the energy density of these systems. Yet, along with the increasing energy density and total capacity of available electrical energy storage systems, potential hazards grow more drastic as well. Uncontrolled energy release in these systems can entail combustion, development of toxic or explosive gases and dusts, or in the worst case, even an explosive failure of the whole energy storage unit. An increasing number of documented incidents with Lithium ion batteries gives evidence of this fact [1–4].

Yet, in spite of obvious safety risks of modern battery systems, an understanding of their complex failure mechanisms and loading limits is not available, for the time being. Accordingly, a systematic investigation of the perilous states of modern electric energy storage systems is highly needed.

Historically, safety studies of lithium-ion batteries were more focused on thermal and electrochemical aspects [5–7]. A series of recent studies over the past five years have investigated the mechanical deformation and onset of short circuit in lithium-ion battery cells. Punch loading has been used as a method of studying internal short circuits in batteries by focusing on thermal response of the cells [8, 9]. In 2012, Sahraei et al [10, 11] and Greve and Fehrenbach [12] reported first measurements of force-displacements in mechanically induced short circuit tests of small pouch cells and cylindrical cells [10–12]. Following that, Jwo Pan and colleagues studied in-plane compressive properties of battery cells and modules of large

pouch cells [13, 14], while Avdeev and Gilaki [15] reported on structural analysis of large cylindrical cells. Most of the above studies and continued research on mechanical characterization of lithium-ion cells and their components were focused on quasi-static testing [16–21].

The only publication reporting on Lithium-ion cell testing at dynamic rates known by the authors is by Jun Xu et al on small cylindrical cells [22]. In vehicle applications of lithium-ion batteries, impact loading is a possible cause of deformation and mechanically induced short circuit [3]. Two common form-factors of batteries used in vehicle applications are large pouch cells and prismatic cells. For example, the Chevrolet Volt battery pack is comprised of large pouch cells [3], while the BMW i3 uses prismatic cells [23]. Therefore, the focus of this study is on experimental investigation of the deformation and subsequent onset of short circuits in lithium ion battery cells of large pouch and elliptical (prismatic) form factors under dynamic loading scenarios.

Regardless of form factor, the interior of battery cells is comprised of a multi-layer system of anode, separator, and cathode sheets, see **Fig. 1**. The order of thickness of those layers are less than 0.1mm. Electrodes (anode and cathode) in turn consist of active particles mixed with polymeric binders and coated on thin aluminum and copper foils. In the case of cylindrical and elliptic (prismatic) cells, the multi-layer system is wound and protected by a hard shell casing of about 0.2 mm thickness, where the casing is commonly made of deep drawn Aluminum of H 3003. In the case of pouch cells, the layers are stacked on top of each other and then wrapped inside a Mylar-like pouch material. Active electrode coatings and separators are porous media soaked in a conductive electrolyte. The constitutive material properties of such a complex system are not easy to explain. However, previous studies have shown that at cell level, the homogenized behavior can be modeled as crushable metallic foams [10, 11, 19].

This paper reports on dynamic punch intrusion tests done over a wide velocity range. In Section 2, the experimental setup and the cells under test will be described in detail. Section 3 gives a description of the test results with elliptic cells and Section 4 follows with results from pouch cells. A preliminary discussion is given in Section 5.

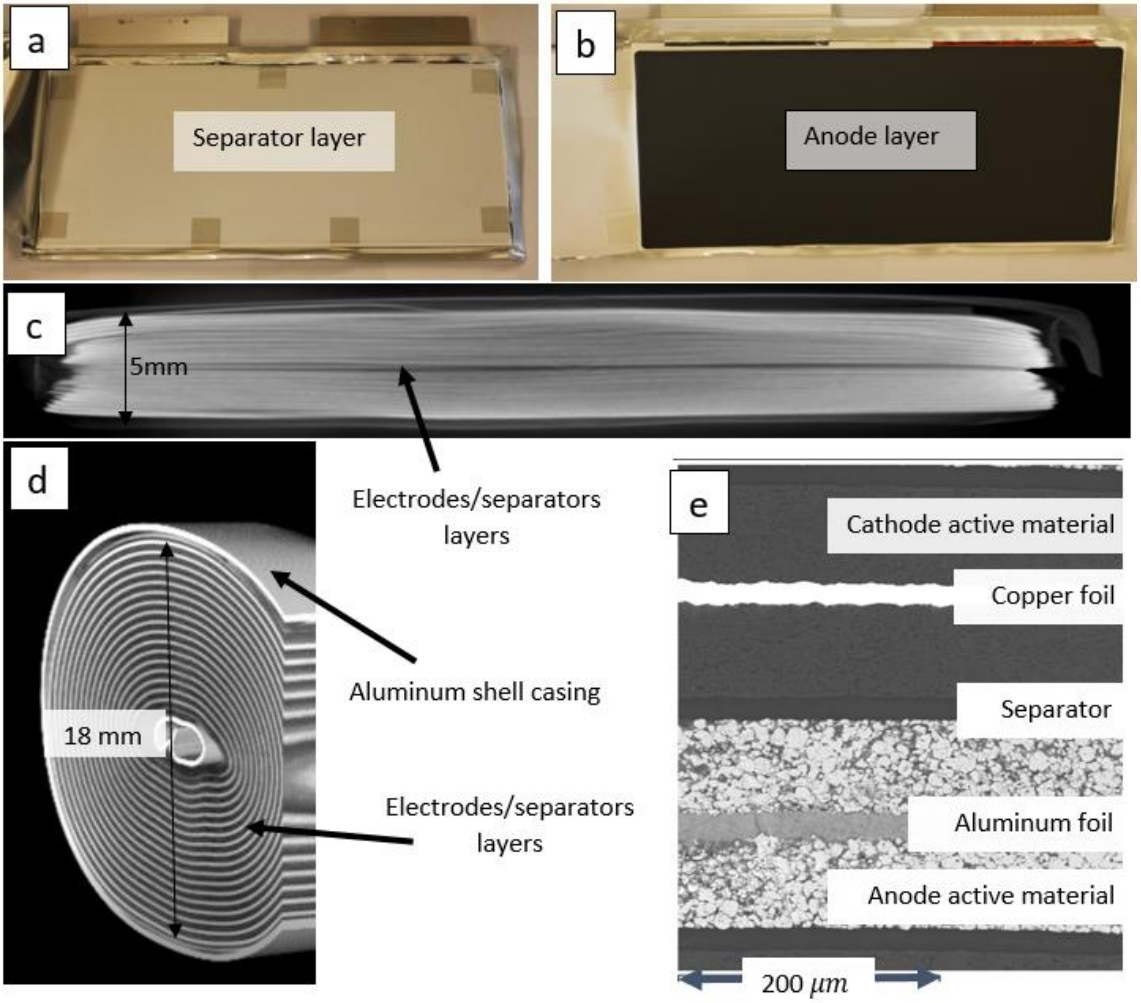


***Fig. 1*** *Interior of battery cells, a) after opening the cover of a pouch cell, the first layer seen is a separator layer, b) the second layer is an anode layer, c) a CT-scan image of a small pouch cell, d) a CT-scan image of a cylindrical cell and e) an SEM image of cross section of electrodes and separators. Figures c,d, and e are courtesy of Exponent Inc [19].*

## 2. Test procedure

### 2.1. Tested battery cells

Lithium-ion cells come in a variety of shapes and sizes. The main cell types in use are cylindrical, elliptical, pouch, and prismatic. Two of these types were tested dynamically on their susceptibility to intrusion: elliptical cells and pouch cells. The elliptical cell with a casing of thin aluminum had dimensions of 37 mm x 64 mm x 18 mm and a capacity of 5.3 Ah. This cell had a nickel oxide chemistry and contained liquid electrolyte. In addition to standard cells filled with electrolyte, inactive cells without electrolyte were tested as well. These cells will be referred to as “dry” cells, in contrast to the normal “wet” cells. Both elliptical cells are identical, apart from the missing electrolyte in the dry specimens.

Two different pouch cells were tested, which will be called pouch A and B. Pouch A had a capacity of 31 Ah, Nickel Manganese Cobalt (NMC) chemistry, and dimensions of 225 mm x 225 mm x 7.2 mm. Pouch B came with a capacity of 52 Ah, a Nickel cobalt oxide chemistry, and dimensions of 329 mm x 161 mm x 12.7 mm.

**Fig. 2** shows photographs of the elliptical cell and the two pouch cells. In preparation of the tests the cells were subjected to at least one full charge/discharge cycle in order to verify its nominal capacity. All tests were done with cells fully discharged (100 % depth of discharge, which means State of Charge (SOC) of 0%). Previous work of same authors have shown the mechanical behavior of batteries before short circuit is not affected by the state of charge [24]. Therefore, it is believed that the discharged state does not affect the validity of the tests while reducing hazards of thermal runaway after the test is completed.

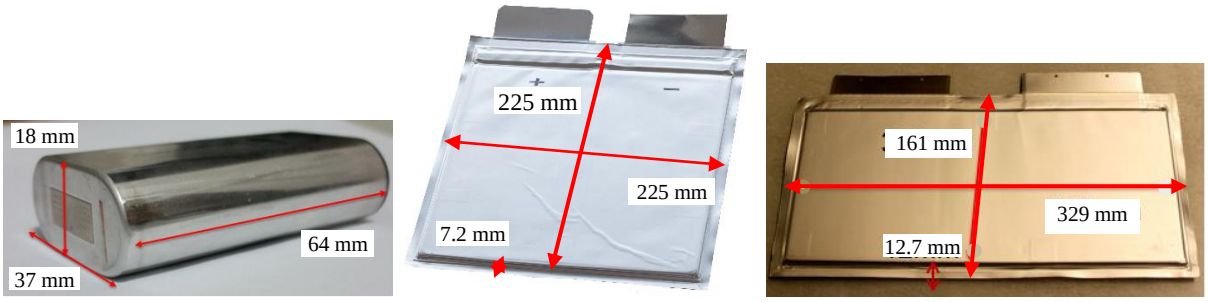


***Fig. 2*** *Elliptic cell, pouch cell A, and pouch B from left to right.*

## 2.2. Experimental setup and test procedure

The test stand is a commercial servo hydraulic machine (Instron 8503, see **Fig. 3**). The machine works with a closed servo loop for cross head velocity. It is able to be operated with cross head velocities between 0.01 mm/s and 5 m/s and a maximum force of 120 kN.

During the tests, the punch's displacement and the intrusion force had to be measured. The punch's displacement was determined from the cross head displacement which is recorded via an inductive transducer integrated in the test stand. For this, a proportionality between the cross head and punch displacements was assumed and elastic test rig deformations were neglected. In view of the rather small forces involved (< 20 kN) this assumption seems reasonable. According to the manufacturer, the error due to a possible deformation of the test rig should not exceed a few tenth of a millimeter while the test stand temperature is maintained constant.

For the determination of the intrusion force a piezo-electric force sensor (Kistler type 9091A) was adapted to the machine. It was pre-loaded to about 10 % of its measurement range between two thick steel pieces one of which contained the punch body (**Fig. 3**, b).The whole setup was first calibrated and then fastened to the cross head of the test machine (**Fig. 3**, b). The punch is 50 mm in length and has a spherical tip with a diameter of 12.7 mm following [10, 21, 25]. This type of punch test is used frequently to characterize material properties of various battery cells for development of finite element models and as a benchmark to compare the response of

various cells. It may represent the intrusion of a bolt head into a battery during the deformation of a battery pack in an electric vehicle.

As cells get short circuited and discharged during the intrusion process, the metallic punch is exposed to charge fluctuations. It is emphasized that no additional disturbances could be found on the force signals during cell penetration and cell discharge. No influence of charge variations on the force measurement could be detected. However, in some cases significant disturbances appeared on the displacement signal during a discharge period. Charge variations on the punch, apparently, could affect the induction process used for displacement measurement. In some rare cases, displacement recordings became almost completely disturbed during the discharge period. Yet, it has to be emphasized that these uncertainties were not present before cell failure. They affect post failure trends only, which are of no importance to the current investigation. Nevertheless, we plan to deploy an electrically decoupled optical system in the future tests for punch displacement measurements. Such system should increase the accuracy of the recordings as well as decouple results from voltage fluctuations in the test specimen.

One difficulty when doing dynamic testing arises from the combination of high punch velocities in conjunction with the small cell thicknesses. As the punch has to penetrate the cells at least some millimeters to generate a short circuit and, additionally, 10-20 millimeters are needed for punch deceleration at higher testing velocities, the punch will penetrate the cell completely and hit the surface beneath with considerable residual speed. This might cause significant damage to the punch and the force sensor. Thus, in order to prevent this, a special setup was devised, called a force limitation device, comprising two metal plates with central holes greater than the punch's diameter, a shear plate and a cylindrical piece of steel (**Fig**. **3**, c). The piece of steel fits into the hole of the upper metal plate and is kept in place by the shear plate beneath. By this, a flat surface is provided for the cells under test. At the same time, the setup provides a limitation for the force exerted onto the punch as the shear plate shears off

when the shearing force (~ 30 kN) is reached. If the force of the punch surpasses the shearing force of the plate, the steel piece falls to the ground and the punch penetrates the cell without further obstruction. This allows the punch to decelerate freely until it stops.

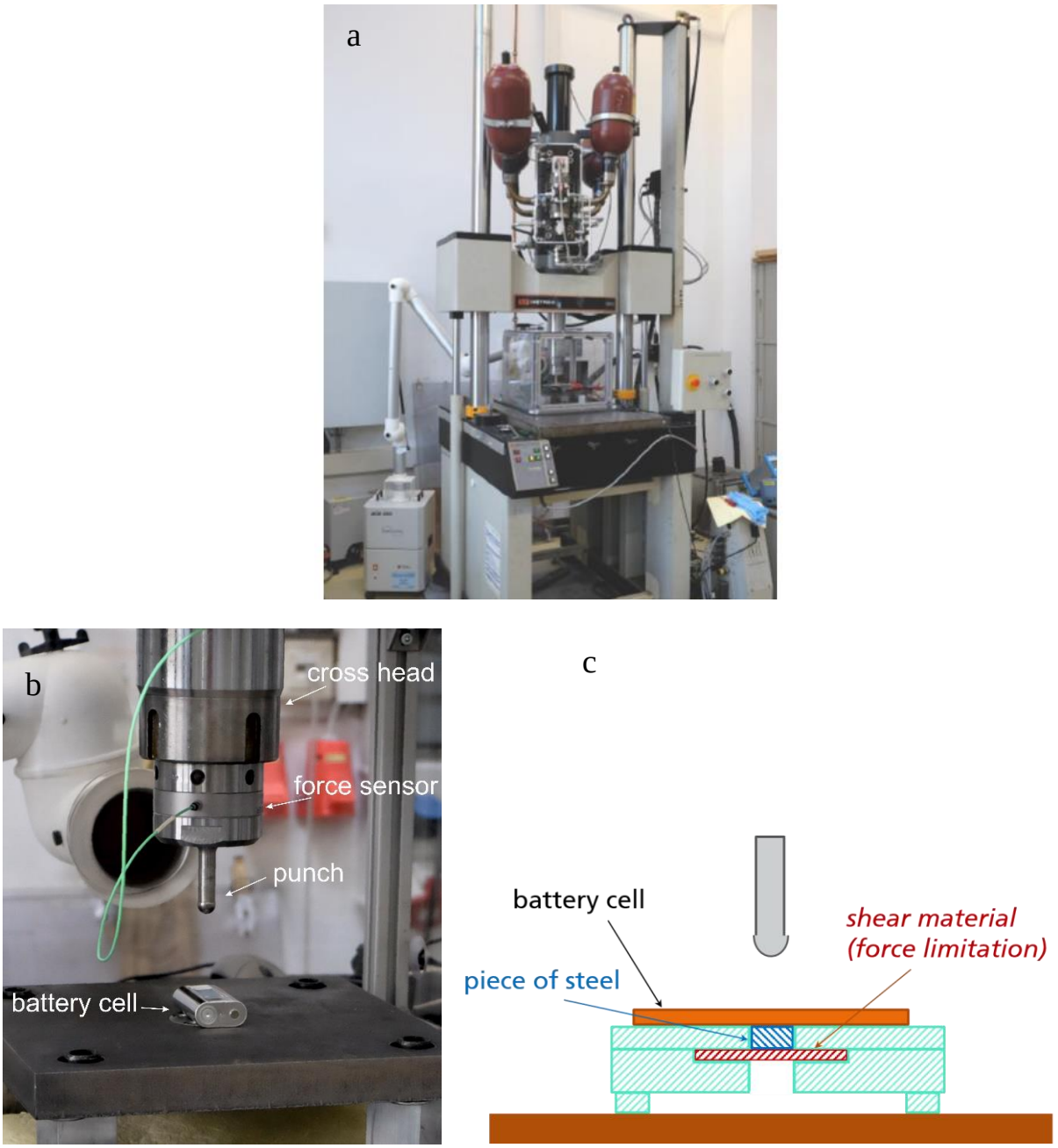


***Fig. 3*** *Experimental setup. a) Commercial servo hydraulic test machine (Instron 8503), b) Photograph with cross head, force sensor, punch, cell, and force limitation device, and c) Drawing showing the inner setup of the force limitation device.*

The shear force is determined by the shear plate thickness and material and can easily be adjusted to lie well above the critical force to be measured and below any destructive value. From quasi static tests the critical force for short circuit generation was known to be around 10 kN [10, 21]. Hence, the shearing force of the punch base device was chosen to be greater than 30 kN, well above the force to be measured. Pieces of steel panel with a thickness of 2 mm were used for this purpose.

It should be pointed out that, as a result of the tests, the cells are usually completely pierced by the punch (**Fig. 4**). Therefore, a post-test analysis of the cells is not possible. **Fig. 4** depicts post-test pictures of some tests, showing on the upper row pierced cells right after tests while still under the punch and on the lower row photographs of cells after removal of punch head.

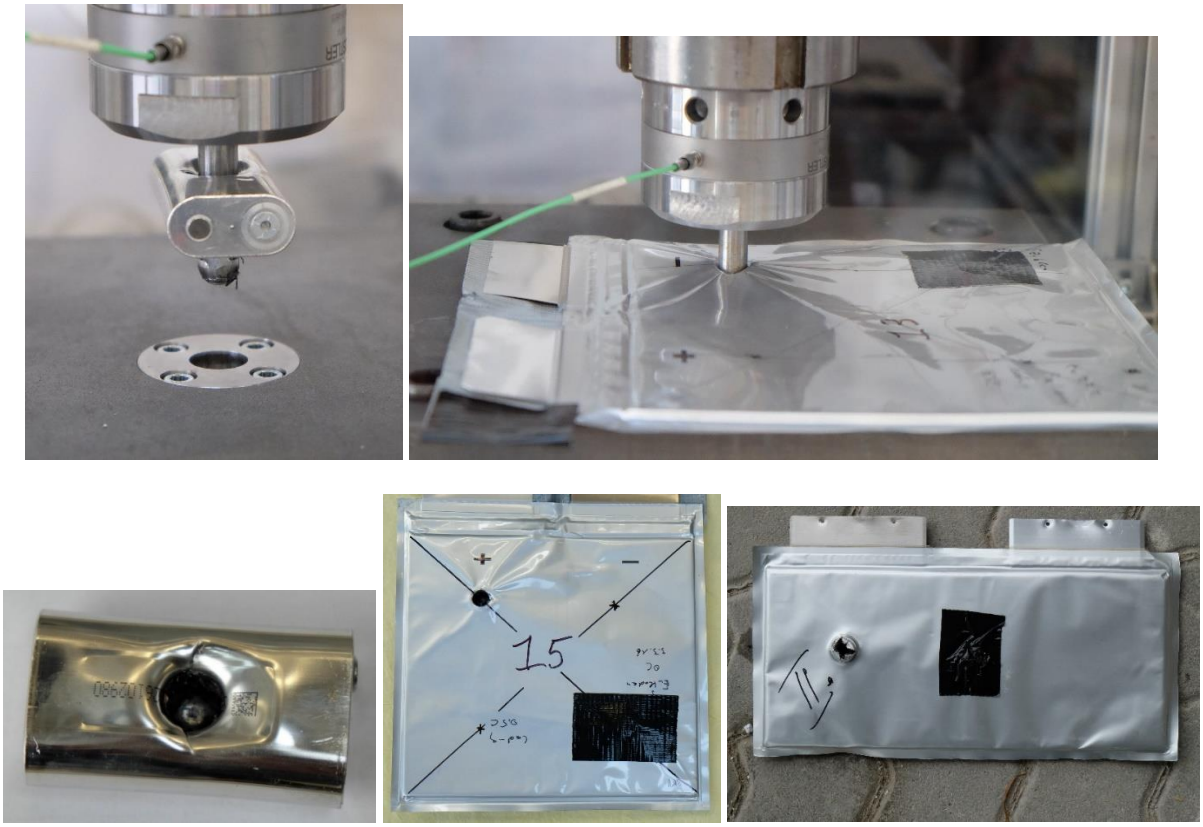


***Fig. 4*** *Posttest photographs of test apparatus and cells. Upper row, from left to right: punch tests of elliptical and pouch cells. Lower row, from left to right: post-test pictures of punctured dry elliptic cell, pouch A, and pouch B.*

## 3. Test results with elliptic cells

During each indentation test, load, displacement and voltage of cell terminals were recorded over time with a transient recorder (MF instruments, TransCom). The recorder allows for data recordings with 12 Bit resolution at a maximum sampling rate of 10 MHz. For the tests sampling rates between 75 Hz and 500 kHz were used, depending on the overall intrusion time which varies with test velocity and cell thickness.

**Fig. 5** depicts recordings from a test with a cross head speed of 5 m/s into a wet elliptical cell. Upon touching the cell surface, the force level increased up to about 8 kN at a displacement of ~ 6 mm, then it broke down to about 5 kN. Upon further penetration of the cell, the load level remained around 6 kN until the back side of the cell was reached. Next, the punch pushed against the back support of the cell and against the shear plate. This finally broke at a load level of ~ 35 kN. The load at this point drops to zero. The punch comes to a rest about 30 mm after having reached the cell surface.

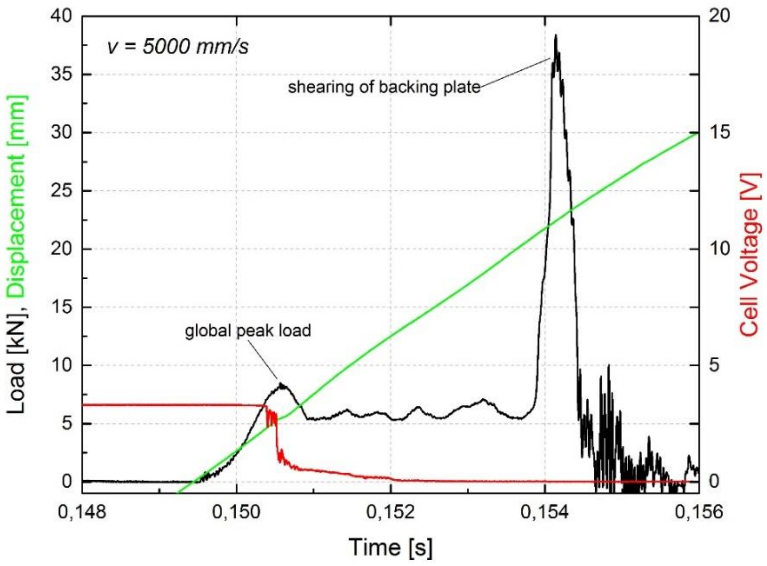


***Fig. 5*** *Load, voltage, and displacement time-histories of a punch test with 5 m/s cross head speed into an elliptical cell.*

The cell failure time, i. e. the onset of short circuit formation, can easily be identified by the drop in voltage. From this, the critical load and critical indentation depth can be determined which are of main importance for investigations of cell failure. Usually, short circuit formation occurs after a few millimeter indentation, and the measurement could be stopped here in principle. Due to the inertia of the punch, however, the punch penetrates further into the cell which usually is completely pierced, as mentioned above. Yet, as only signals up to the failure time are of importance, only the first part of the signal histories will be shown in the rest of this paper.

The results of a test are most intuitively presented as load displacement curves where the load is displayed as a function of indentation depth. For preparing these curves the measured cross-head displacement, assumed to be proportional to the indentation depth, was carefully set to zero at the punch's impingement time on the cell which was determined by the rising edge of the load time history.

**Fig. 6** depicts two such curves from tests with different velocities. On the left side, the test results from **Fig. 5** are drawn again around the failure time. Voltage here starts to decrease at about 4.5 mm indentation when the load is still increasing. The global load maximum is reached at about 5.5 mm indentation. This indentation coincides with a sharp drop of the voltage which goes to zero afterwards.

On the right side of **Fig. 6** a test with cross head speed of 1 mm/s is depicted. It can be seen that the critical load level is almost identical, the indentation depth is slightly increased.

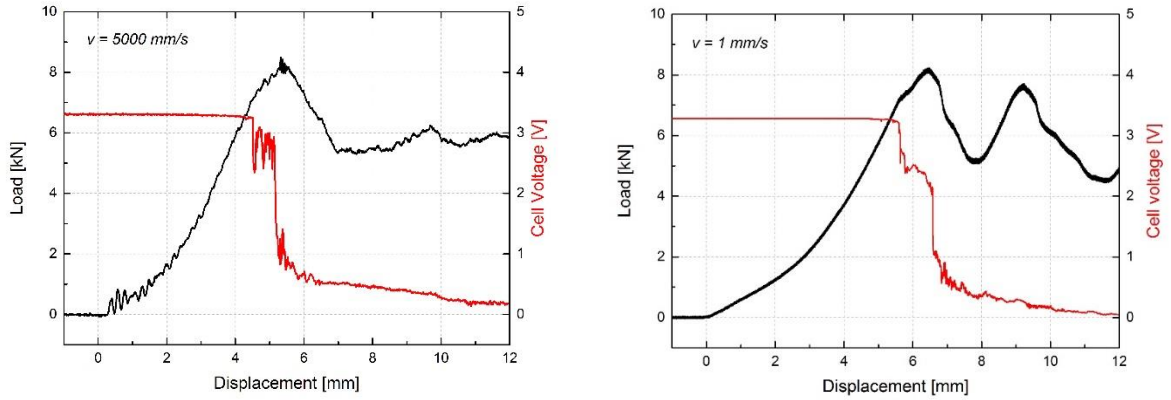


***Fig. 6*** *Load and voltage-displacement curves of two indentation test with wet elliptic cells at different velocities.*

The failure mode seen in **Fig. 6** (failure mode I), consisting of a minor voltage drop before load maximum and a more pronounced drop at load maximum, is typical for most of the wet elliptical cells. At high velocities (> 10 mm/s) this was the only failure mode observed. Yet at lower velocities, a second failure mode occurred in some tests (mode II). In these cases, the voltage dropped sharply to zero, coinciding with a small drop in force, well in advance of the global load maximum (cp. **Fig. 7**) which is reached after a couple of millimeters additional displacement. Apparently, a strong internal short is formed before the global load maximum is reached.

It is not clear what factor drives the cell to either failure mode. The occurrence of mode I or II failure seemed to be more a matter of probability. **Fig. 7**, right side, presents load and voltage displacement curves for two identical tests performed with 0.1 mm/s. In one test the cell failed in mode I, the other in mode II. We want to emphasize the reproducibility of the load displacement measurements clearly seen in the figure up to the point of failure. It is interesting that the voltage starts to decrease in both failure modes at a load of approximately 4.5 kN and an indentation depth of slightly below 5 mm. However in mode II it drops immediately to zero,

with just a small drop in force, while in mode I the most significant drop in voltage occurs after the global load maximum.

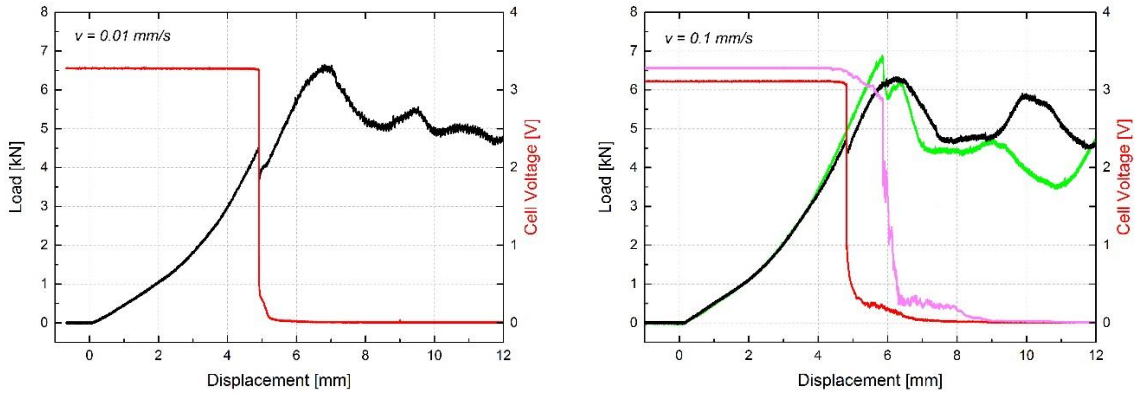


***Fig. 7*** *Load displacement and voltage of a punch test with 0.01 mm/s cross head speed, left side, and 0.1 mm/s, right side, into a wet elliptical cell.*

From the tests of wet elliptic cells, up to three specific load and indentation levels can be extracted: the levels at initial voltage drop (soft short), the levels at complete voltage break down (hard short), and the levels at global load maximum. In **Fig. 8** these three load levels are depicted as a function of test velocity for the nine wet cells tested. Clearly, every test yields a hard short and a global peak load. Additionally in failure mode I, a soft short level can be determined. Furthermore, in failure mode I, in most cases, the global peak load almost coincides with the formation of a hard short circuit which forms when the cell starts to be penetrated. From the three points of hard short circuit in the lower region of **Fig. 8** three cells were observed to fail exhibiting failure mode II.

Analyzing short circuit formation from tests with velocities greater than 1 mm/s involves significant uncertainties due to the small time scales involved. As the whole indentation process takes some milliseconds or less in the high dynamic range, precisely discriminating the formation point of any short circuit or even discriminating between soft and hard short circuits

is difficult and apt to misinterpretation, especially as discharging of a cell takes milliseconds to be completed even with a hard short circuit. For example, looking at **Fig. 7**, all clearly discernibly hard short circuits needed more than 5 milliseconds for discharging. This amounts to only a small fraction of the indentation period for the low velocities shown in **Fig. 8**, but increases to almost the complete indentation time for the highest velocities tested. Hence in the high dynamic range, a soft short circuit is not easily detected and might be overlooked due to the very small voltage drop in the limited observation time between soft short and global failure. Moreover, higher vibration levels of the test stand and hence a decreasing signal to noise ratio add further ambiguity. This is pictured in the increasing scatter of the short circuit data at higher velocities in **Fig. 8**.

The overall and important result remains unaffected by any uncertainty of soft short determination, namely that there exists a risk for a short circuit at indentation depths approximately 2 mm smaller than the one necessary for global failure. The upper dotted line in **Fig. 8** is a least square fit to the points of load maximum, which can be determined unambiguously for the complete velocity range. The lower line is a parallel line meant as guide to the eye. It is interesting to see that the three points of hard short circuit from failure mode II are in line with the points of soft short circuit for failure mode I (see **Fig. 7** right side).

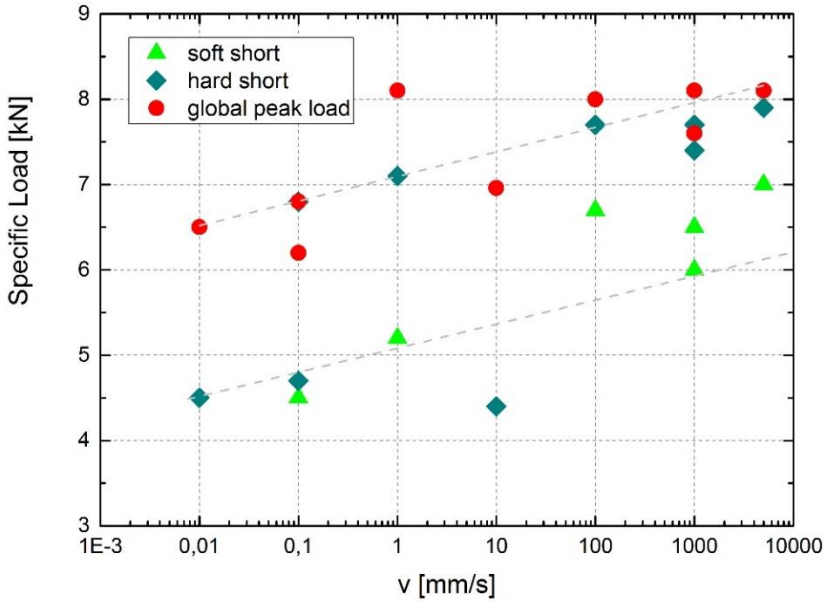


**Fig. 8** *Measured specific load levels for soft short circuit, hard short circuit, and global peak load for wet elliptic cells.*

In **Fig. 9** load displacement histories of dry cells are depicted. Here, of course, no voltage signal is available. The force signal itself looks similar to the wet cells. Yet the first force maximum is significantly higher than with the wet cells. There are also differences in the slope of the load signal and the dependence on the test velocity.

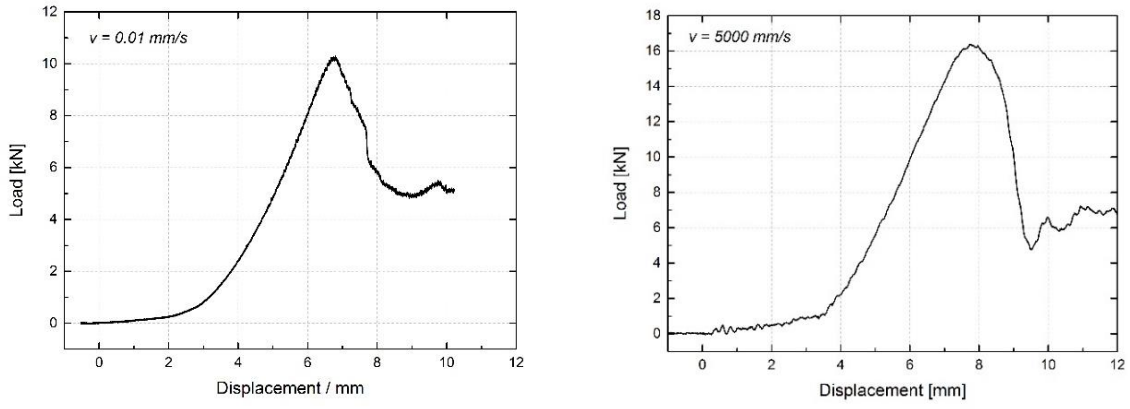


***Fig. 9*** *Force-time histories of a dry cell.*

From the nine tests done with dry cells the global maximum in load and the respective indentation depth was extracted. The results for global force maximum are plotted in **Fig. 10** as a function of indentation velocity together with the results of the wet cells, already shown in **Fig. 8**. Compared to the wet cells the dry cells do not only exhibit a higher force level, they also show a higher dynamic change. In fact the force maximum of the dry cells increases by about 60 % over the tested velocity range. For the wet cells the observed increase is only ~ 25 %. It is observed that the inner liquid significantly increases the susceptibility of the cell to mechanical failure.

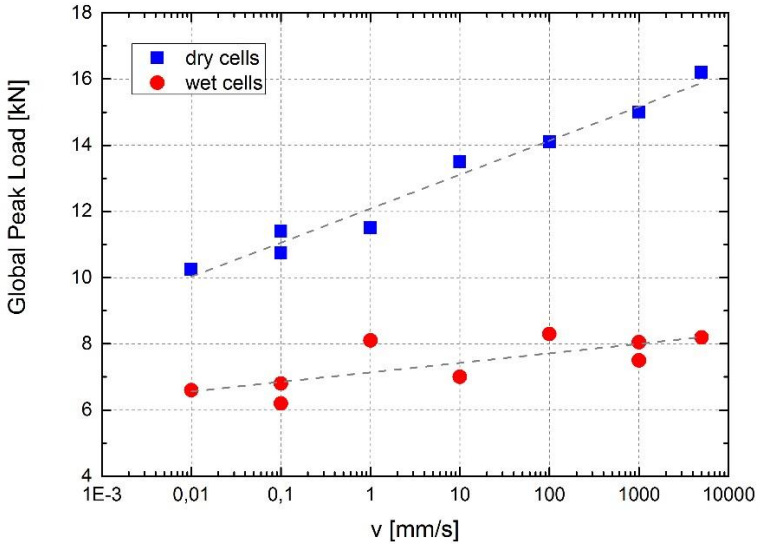


***Fig. 10*** *Summary of results with elliptic cells. The lines are least square fits to the data points.*

As to the indentation depth, **Fig. 11** depicts load-displacement curves for different velocities for both dry and wet elliptical cells. It can be seen that for the dry cells, the higher the velocity the deeper is the indentation into the cell without much change to the slope of the load

displacement curve. Although no significant strain rate hardening occurs, the critical force significantly increases at higher velocities.

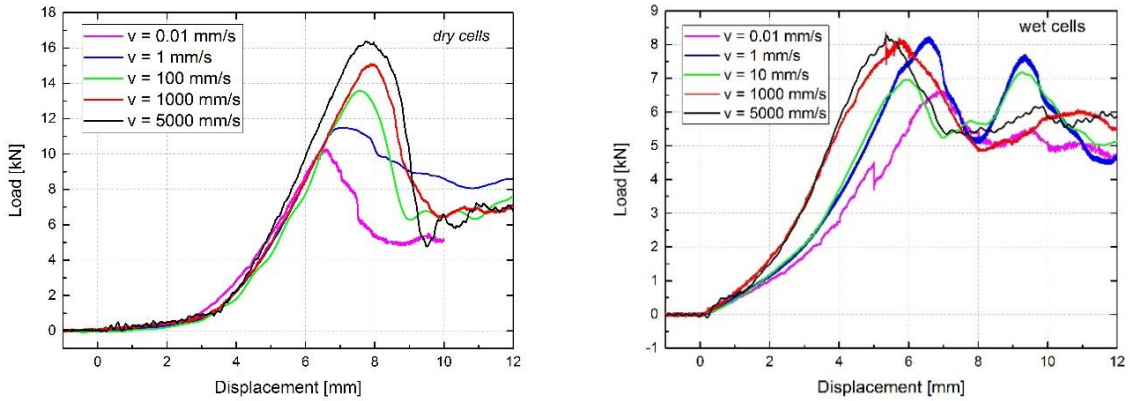


***Fig. 11**: Load displacement curves for dry and wet elliptic cells for different punch velocities.*

For the wet cells, the situation is different. With increasing velocity, the load displacement curves exhibit an increasing slope as well as a decreasing indentation depth to failure. These effects together result in the rather flat dependence of the critical force on velocity (**Fig. 10**). Nevertheless, the hardening effects for the slope of the curves in wet cells is higher than in the case of the dry cells with a stronger dependence of critical force on velocity.

The indentation depth at the global peak load as a function of punch velocity, is depicted in **Fig. 12**. Although the scatter in the data is rather large, the increasing trend of the critical load in the case of the dry cells and the decreasing trend of critical load in the case of the wet cells is evident. The dotted lines in the figure are least square fits to the data points and are added as a guide. The data seem to indicate that at very slow velocities ($v << 1$ µm/s), the liquid is simply drawn aside during the indentation process and has no influence on the failure mechanism, while it does have an effect at higher velocities.

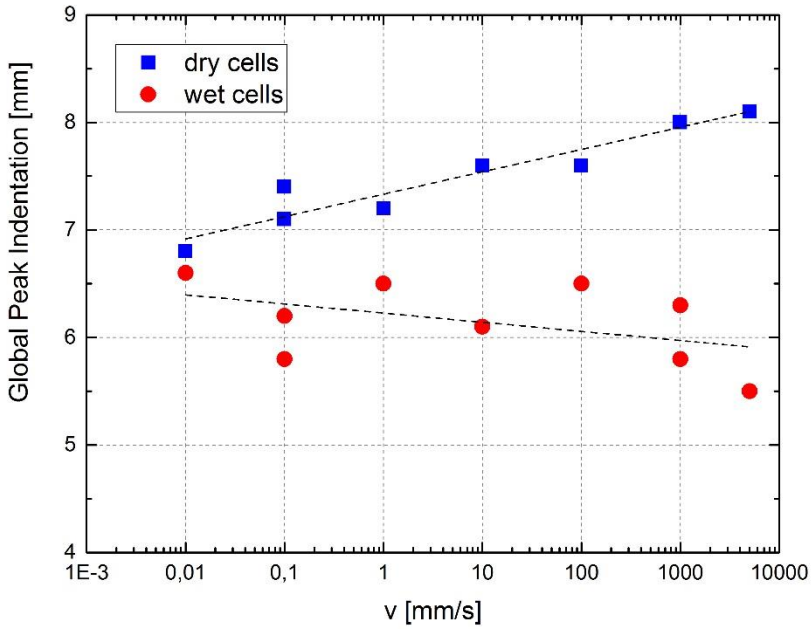


***Fig. 12*** *Critical indentation depth as function of velocity for the elliptic cells. The lines are least square fits to the data points, they cross at a velocity of about 1.5 µm/s.*

## 4. Test results with pouch cells

Testing of the pouch cells was done in exactly the same way as with the elliptic cells. Load displacement curves qualitatively look similar, even though, due to their smaller thickness (approximately 1/3 of the thickness of the elliptic cells) and the lack of a housing, critical indentation depths are significantly smaller. Yet some principal differences exist. Firstly, no significant voltage decrease was observed before the global load maximum. It is upon puncturing of the cell that the voltage starts to decline. Secondly, there were several cases where the voltage did not drop to zero during a test. Rather the voltage remained at a slightly lower level. Therefore, it is possible to pierce a pouch cell without causing a complete short circuit. As with the elliptic cells, there were cases with a single sharp drop in voltage and others with only a gradual decrease. **Fig 13** presents examples of test results for different velocities.

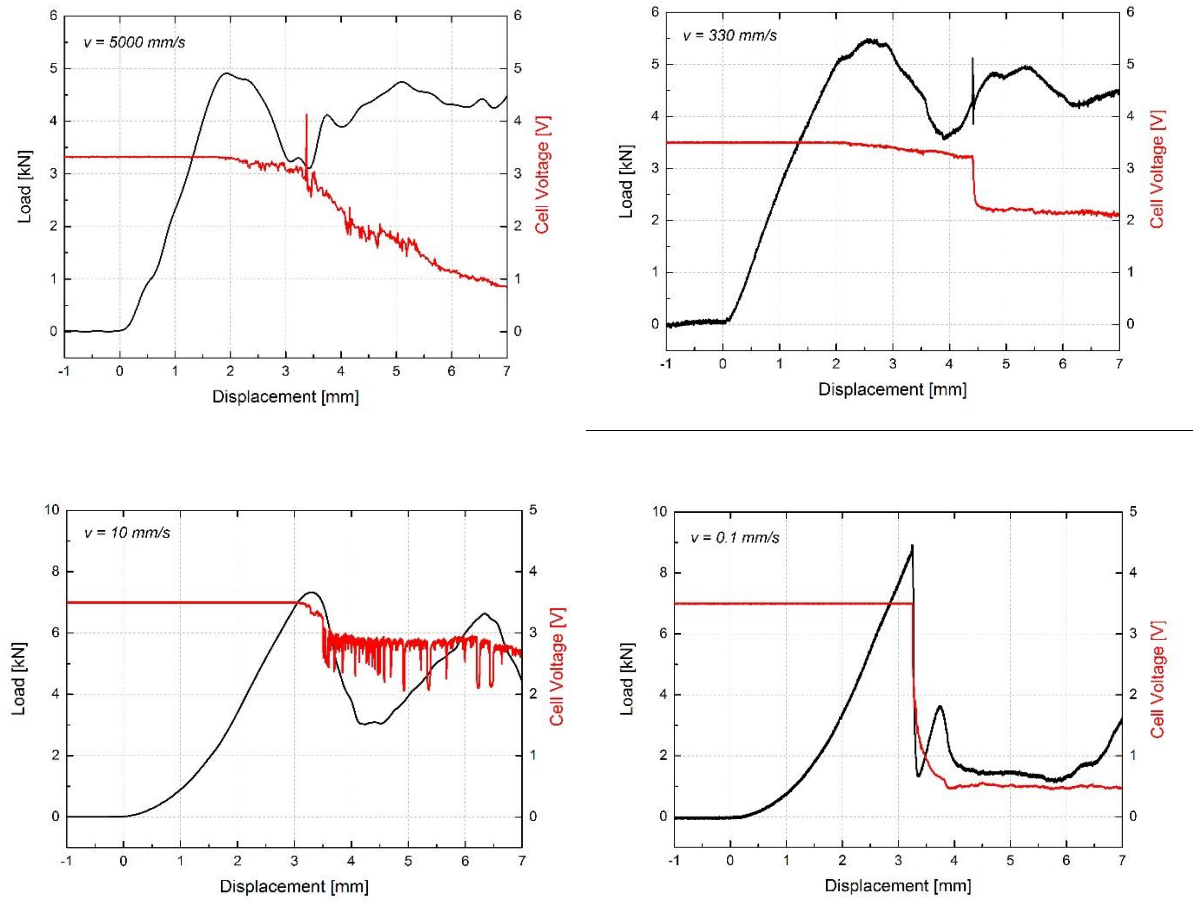


***Fig 13*** *Load and voltage-displacement curves of indentation tests with pouch cells of type A at different velocities*

In order to increase the number of data points, several tests were performed on each pouch cell. This was possible due to the large area of the pouch cells, so each cell could be pierced several times without interference between the different measurement areas. Of course, voltage and short-circuit information could only be registered with cells not being short-circuited. Therefore, usually only one test per cell allowed a voltage-time history to be measured. Further tests, done with cells already short-circuited, provided load displacement recordings, only. This however does not constitute a significant disadvantage as the load maximum is the only important force level for the pouch cells. Up to four tests with a single pouch cell of type A and up to three with type B were done.

No significant differences in the load displacement curves of a new pristine cell and cells short circuited by a former test were found, at least not up to the time of the global load maximum. **Fig. 14** gives the load displacement curves of two tests performed with v = 1 mm/s. The sharp voltage drop in the case of the pristine cell is accompanied by a sharp drop in load while the drop in force is more gradual in the case of the previously short circuited cell. Yet, the rising edge of the curve and the peak load are almost identical.

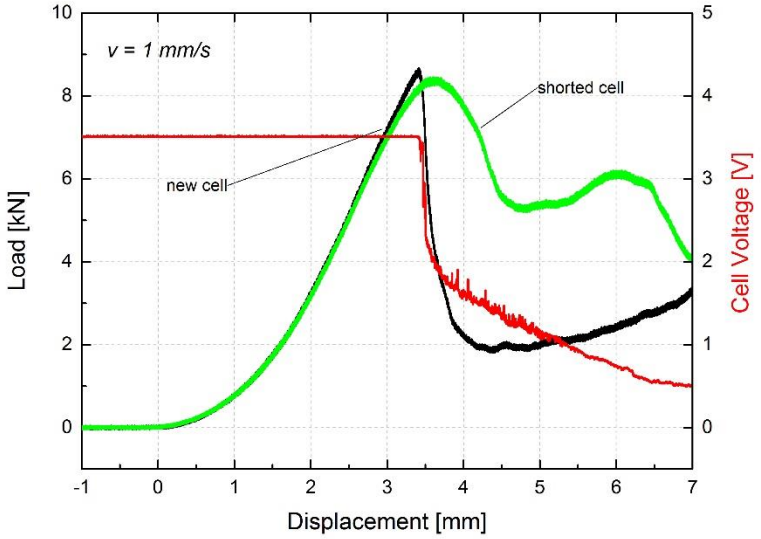


***Fig. 14*** *Load displacement curves for two tests both with v = 1 mm/s.*

Four cells of each type of pouch cell were available for testing. 16 tests with type A and 11 with type B cells were done. All tests have been evaluated as to the load and indentation depth at global load maximum, this was the only point of interest for pouch cells, as soft shorts were not observed for these cells. **Fig. 15** depicts the results for the load maximum as a function of velocity for both kinds of tested pouch cells. The two types of pouch cell show similar behavior. The global load drops by a factor of approximately two in the tested velocity range. All results made with active cells, i.e. cells with a voltage signal, are marked with a cross. Note that five measurements from each cell type could be performed with an active voltage signal because in

each case one cell did not develop a permanent short-circuit in the first test and could be used with voltage signal a second time.

Comparing the global load of elliptical and pouch cells (**Fig. 10** and **Fig. 15**), it is interesting to note that the critical load for the pouch cells is higher in the low velocity range but lower in the high velocity range. Hence, they offer higher safety in a quasi-static impact scenario but less in a dynamic one than elliptic cells.

In **Fig. 16** the measured indentation depth at global load maximum is shown as a function of velocity. The indentation depth decreases by a factor of approximately two as well. The two dotted lines again are least square fits to the data points. The two fits result in almost identical slopes for both kind of pouch cells. Yet, the absolute values of critical indentation for pouch B are about one millimeter higher than the ones for pouch A. This probably is related to different thicknesses of the cells, considering that pouch cell A was about 60 % thinner than pouch cell B.

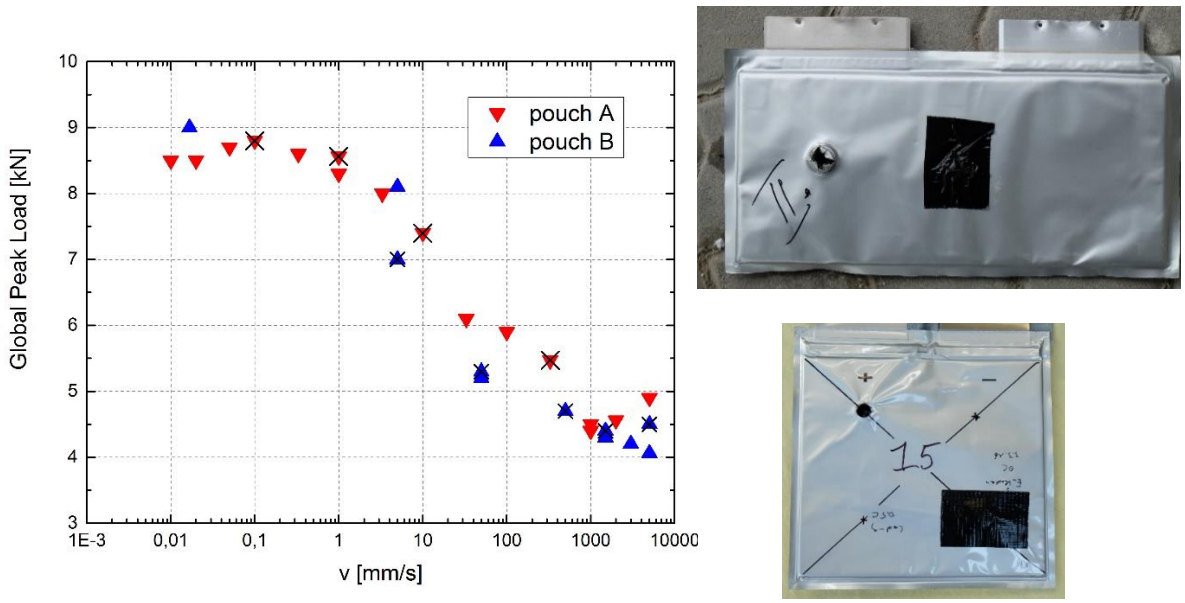


***Fig. 15*** *Critical load for both types of pouch cell tested. Tests made with active cells are marked with a cross. The other tests were made with cells already short-circuited from former testing.*

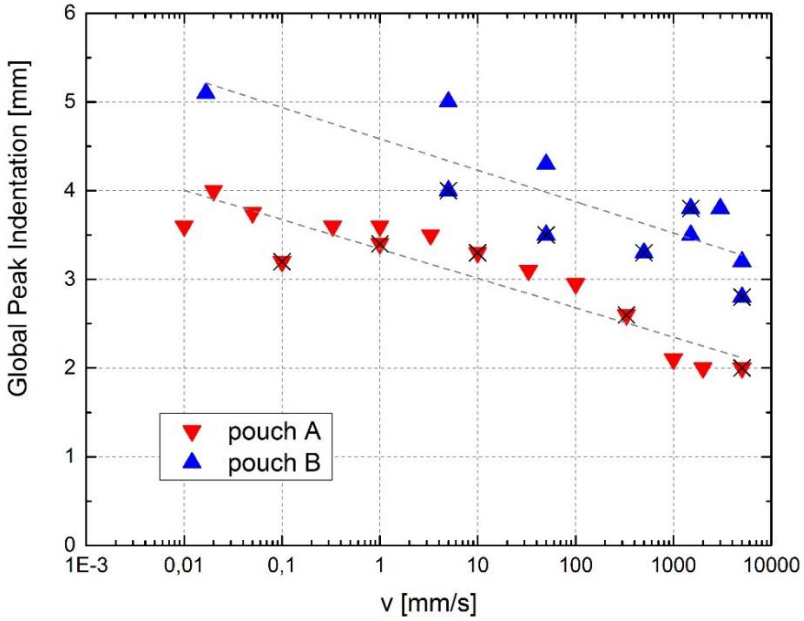


***Fig. 16*** *Indentation depth as function of velocity for dry elliptic cells and both kinds of pouch cell. Tests made with a fresh pristine cell are marked with a cross. The other pouch cell tests were made with an already short-circuited cell from former testing. The lines are least square fits to the data points.*

In **Fig. 17** load displacement curves from different test velocities with pouch A cells are presented. These cells seem to harden at higher velocities as the curves steepen with increasing velocity. Yet, as the brittleness increases with speed, the critical indentation depth and the critical load decrease.

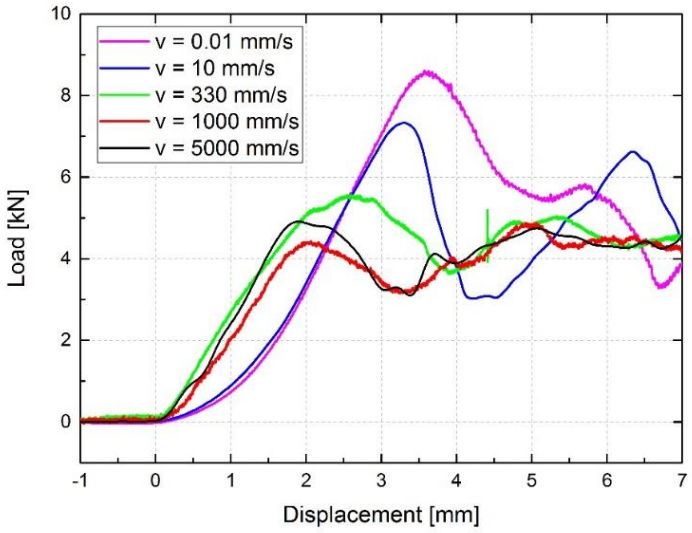


***Fig. 17*** *Load displacement curves for pouch cells of type A for different punch velocities.*

## 5. Discussion on failure modes

Initial investigations of our group involving tensile tests on battery components have shown strain rate hardening and reduced ductility at higher speeds [26]. The strain rate hardening observed in the tests could be explained by the strain rate hardening of the components used in the battery cells and for their casings. The interior layers of aluminum and copper foils and polymeric separators are all materials that exhibit strain rate hardening, so is the hard aluminum casing of the elliptical cells and Mylar-like pouch materials of pouch cells. In the case of wet cells, the hydrostatic pressure and viscosity of the liquid electrolyte also adds to this effect. The final peak force is determined by these two competing effects: strain rate hardening and reduced ductility at higher speeds. In the case of elliptic cell, the strain rate hardening is stronger than the reduced ductility effects at higher speeds and overall the peak force increases. However, in pouch cells, the brittleness of material at higher speeds is stronger than the strain rate hardening effects and this results in a lower peak force in dynamic velocities.

The reduction of peak force in wet cells compared to dry cells can be explained by the effects that electrolyte has on the polymeric separators. It has been shown that the strength of the polymeric separators decreases when they are soaked in dimethyl carbonate (DMC) which is the main component of the electrolyte used in lithium-ion batteries [27]. Furthermore, molecular dynamic simulations indicate that DMC molecules absorbed in amorphous sections of polymeric separators result in loss of Young's modulus [28]. Considering that the peak force and the onset of short circuit are controlled by a failure of the separator, these effects explain why wet cells have lower critical loads.

The observations in this study of two failure modes in the elliptical cell can be explained by the theory of soft and hard internal short formation due to mechanical loading of separators as explained by Zhang et al 2016 [20]. In that publication, the authors studied failure of dry processed separators under biaxial punch loading. They observed that two failure modes exist for these anisotropic separators, one leads to a large sudden slit along Machine Direction (MD) and the other to a smaller opening along Transverse Direction (TD) of the separator. In the first failure mode, called mode A, a separator under punch loading ruptures when TD loading reaches a critical level and suddenly a large slit is formed. While, under second failure mode, mode B, the separator becomes thin and transparent, but does not rupture when the critical TD loading value is reached; in fact deformation of the separator continues until loads reach the critical limit in MD, which is a relatively higher value and then a small crack is formed. Therefore, the mode A failure is a one-step failure which immediately causes a large contact area between anode and cathode, and leads to a hard short circuit. On the other hand, in failure mode B, the first step of failure is thinning of the separator, which starts at the same critical load as mode A, and it is not expected to create a total short circuit, but only a soft short indicated by a slight decrease in voltage. The second step in failure mode B is the formation of a small crack at a higher load. It is at that point that finally a hard short circuit forms. The two separator failure modes are shown in **Fig. 18**.

The two types of failure observed in elliptical cells (as shown in **Fig. 7** right) are consistent with these two failure modes in dry processed separator failures. In elliptical cell failure mode I, a decrease in voltage precedes the global peak in load and complete loss of voltage by 1 mm, which is consistent with failure mode B in the separator. The elliptical cell failure mode II is characterized by a sudden total drop in voltage which is a characteristic expected in failure mode A of the separator.

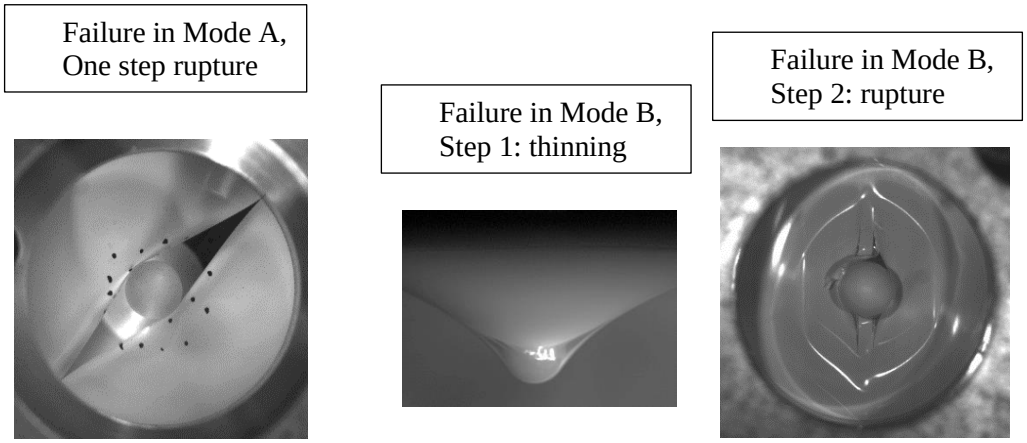


***Fig. 18*** *Failure of dry processed separator in Modes A and B [20].*

The drops in force during a soft or hard short can have different causes. A fracture in layers of electrode/separator assembly, a fracture in shell casing, or loss of stiffness due to discharge are three possible phenomena contributing in drop or gradual reduction of force. For elliptical cells, a notable local drop in force generally coincides with the voltage drop in mode II. Yet similar drops also appear in many tests in failure mode I when the hard short forms (cp. **Fig. 7,** green curve). Besides fracture of few layers, another explanation for this drop is a reduction of cell stiffness during discharge [24, 25]. It is visible most pronouncedly at low indentation velocities where the time scale of discharge (some milliseconds) is fast compared to the indentation process (see also lower right of **Fig 13** and **Fig. 14**). The global peak load also indicates that the metal shell casing of the elliptical cell has been punctured.

## 6. Summary and conclusion

Dynamic local indentation tests have been performed in the velocity range between 0.01 mm/s and 5 m/s. With two different types of pouch cells, it was demonstrated that the critical force necessary to generate an internal short, defined as first force maximum in the load displacement curves, drops roughly by a factor of two from about 8 kN to about 4 kN in the tested velocity range. The apparent strain rate effect of decrease in critical load is an interesting feature of the dynamic response of pouch cells. It is both counter intuitive and difficult to explain. An explanation of this phenomenon at the micro mechanical level is the subject of the ongoing research.

With the tested elliptic cells, the behavior was quite different. Here the critical force increased in the case of wet cells and dry cells. In the tested dynamic range the increase was by ~ 25 % with wet elliptic cells and ~ 60 % with dry elliptic cells. It was found with the wet cells that the voltage drop often starts before the force maximum was reached. Different failure modes were found which are consistent with two failure modes observed at dry processed separators. The observed strain rate hardening behavior for elliptical cells is consistent with the known response of metallic and polymeric materials subjected to dynamic loading.

These findings are important for a realistic evaluation of battery crash safety, as they indicate that the failure limit of battery cells should be estimated in dynamic rather that quasi-static tests.

## Acknowledgements

We gratefully acknowledge the help of Matthias Bruder, Quirin Kolb, and Jürgen Bauer in preparing the tests. This work was partially supported by the MIT Battery Consortium.

## References

[1] Wang Q, Ping P, Zhao X, Chu G, Sun J, Chen C. Thermal runaway caused fire and explosion of lithium ion battery. J Power Sources 2012;208:210–24. doi:10.1016/j.jpowsour.2012.02.038.

[2] Willard N, He W, Hendricks C, Pecht M. Lessons Learned from the 787 Dreamliner Issue on Lithium-Ion Battery Reliability. Energies 2013:4682–95. doi:10.3390/en6094682.

[3] Smith B. Chevrolet Volt Battery Incident Overview Report. 2012.

[4] BBC. Authorities investigate after Tesla car catches fire. BBC News Technol n.d. http://www.bbc.com/news/technology-37104753 (accessed March 12, 2016).

[5] Kim G-H, Pesaran A, Spotnitz R. A three-dimensional thermal abuse model for lithium-ion cells. J Power Sources 2007;170:476–89. doi:10.1016/j.jpowsour.2007.04.018.

[6] Spotnitz RM, Weaver J, Yeduvaka G, Doughty DH, Roth EP. Simulation of abuse tolerance of lithium-ion battery packs. J Power Sources 2007;163:1080–6. doi:10.1016/j.jpowsour.2006.10.013.

[7] Abada S, Marlair G, Lecocq A, Petit M, Sauvant-Moynot V, Huet F. Safety focused modeling of lithium-ion batteries: A review. J Power Sources 2016;306:178–92. doi:10.1016/j.jpowsour.2015.11.100.

[8] Maleki H, Howard JN. Internal short circuit in Li-ion cells. J Power Sources 2009;191:568–74. doi:10.1016/j.jpowsour.2009.02.070.

[9] Cai W, Wang H, Maleki H, Howard J, Lara-Curzio E. Experimental simulation of internal short circuit in Li-ion and Li-ion-polymer cells. J Power Sources 2011;196:7779–83. doi:10.1016/j.jpowsour.2011.04.024.

[10] Sahraei E, Hill R, Wierzbicki T. Calibration and finite element simulation of pouch lithium-ion batteries for mechanical integrity. J Power Sources 2012;201:307–21. doi:10.1016/j.jpowsour.2011.10.094.

[11] Sahraei E, Campbell J, Wierzbicki T. Modeling and short circuit detection of 18650 Li-ion cells under mechanical abuse conditions. J Power Sources 2012;220:360–72. doi:10.1016/j.jpowsour.2012.07.057.

[12] Greve L, Fehrenbach C. Mechanical testing and macro-mechanical finite element simulation of the deformation, fracture, and short circuit initiation of cylindrical Lithium ion battery cells. J Power Sources 2012;214:377–85. doi:10.1016/j.jpowsour.2012.04.055.

[13] Lai W-J, Ali MY, Pan J. Mechanical behavior of representative volume elements of lithium-ion battery cells under compressive loading conditions. J Power Sources 2014;245:609–23. doi:10.1016/j.jpowsour.2013.06.134.

[14] Ali MY, Lai W-J, Pan J. Computational models for simulations of lithium-ion battery cells under constrained compression tests. J Power Sources 2013;242:325–40. doi:10.1016/j.jpowsour.2013.05.022.

[15] Avdeev I, Gilaki M. Structural analysis and experimental characterization of cylindrical lithium-ion battery cells subject to lateral impact. J Power Sources 2014;271:382–91. doi:10.1016/j.jpowsour.2014.08.014.

[16] Zhang X, Sahraei E, Wang K. Deformation and failure characteristics of four types of lithium-ion battery separators. J Power Sources 2016;327:693–701. doi:10.1016/j.jpowsour.2016.07.078.

[17] Sahraei E, Bosco E, Dixon B, Lai B. Microscale failure mechanisms leading to internal short circuit in Li-ion batteries under complex loading scenarios. J Power Sources 2016;319:56–65. doi:10.1016/j.jpowsour.2016.04.005.

[18] Zhu J, Zhang X, Sahraei E, Wierzbicki T. Deformation and failure mechanisms of 18650 battery cells under axial compression. J Power Sources 2016;336:332–40. doi:10.1016/j.jpowsour.2016.10.064.

[19] Sahraei E, Kahn M, Meier J, Wierzbicki T. Modelling of cracks developed in lithium-ion cells under mechanical loading. RSC Adv 2015;5:80369–80.

[20] Zhang X, Sahraei E, Wang K. Li-ion Battery Separators, Mechanical Integrity and Failure Mechanisms Leading to Soft and Hard Internal Shorts. Nat Sci Reports 2016. doi:10.1038/srep32578.

[21] Sahraei E, Meier J, Wierzbicki T. Characterizing and modeling mechanical properties and onset of short circuit for three types of lithium-ion pouch cells. J Power Sources 2014;247:503–16. doi:10.1016/j.jpowsour.2013.08.056.

[22] Xu J, Liu B, Wang X, Hu D. Computational model of 18650 lithium-ion battery with coupled strain rate and SOC dependencies. Appl Energy 2016;172:180–9. doi:10.1016/j.apenergy.2016.03.108.

[23] Moloughney T. Here's Why an i3 Battery Upgrade Currently Doesn't Make Sense. Electr BMW i3 2016:1–2. http://bmwi3.blogspot.com/2016/05/heres-why-i3-battery-upgrade-currently.html (accessed June 3, 2017).

[24] Meier JD, Sahraei E, Salk M, Kisters T, Huberth F. State of Charge vs . Thermal Runaway for Lithium Ion Large Pouch Cells. Batter. Congr., 2013.

[25] Wierzbicki T, Sahraei E. Homogenized mechanical properties for the jellyroll of cylindrical Lithium-ion cells. J Power Sources 2013;241:467–76. doi:10.1016/j.jpowsour.2013.04.135.

[26] Zhang X. Mechanical Behavior of Shell Casing and Separator of Lithium-ion Battery. Massachusetts Institute of Technology, 2017.

[27] Sheidaei A, Xiao X, Huang X, Hitt J. Mechanical behavior of a battery separator in electrolyte solutions. J Power Sources 2011;196:8728–34. doi:10.1016/j.jpowsour.2011.06.026.

[28] Yan S, Xiao X, Huang X, Li X, Qi Y. Unveiling the environment-dependent mechanical

properties of porous polypropylene separators. Polym (United Kingdom) 2014;55:6282–

92. doi:10.1016/j.polymer.2014.09.067.